Table 3. L-Phe as starting material. Concentrations: 500 μmol Phe, 8.5 mmol $Mg(OH)_2$,1 mmol $FeSO_4$, 1 mmol $NiSO_4$, and 3 mmol Na_2S; 1 bar CO charged after 0, 4, 20, and 44 hours.

Time (hours)	pH	Phe-Phe (D)		Urea (F)		Hydantoin (E) all isomers (μmol)
		LL + DD (μmol)	DL + LD (μmol	LL + DD (μmol)	DL + LD (μmol)	
0.5	9.5	4	—	4	—	—
1	9.5	5	—	5	—	—
2	9.4	18	—	7	—	—
4	9.4	20	—	9	—	2
20	9.5	29	—	11	—	4
44	9.9	32	2	15	1	7
120	9.7	29	8	18	5	14

We previously considered two possibilities as activated α-amino acid: an *N*-carboxy-amino acid anhydride or an oxazolidinone (*1*). We now tentatively favor the *N*-carboxy-amino acid anhydride, because so far in the reaction of Phe to Phe-Phe we have not detected *N*-formyl-Phe-Phe. *N*-carboxy-amino acid anhydrides are well known to form peptides in aqueous systems through *N*-carbamoyl peptides (*3*). In the experiments starting with L-Phe, we confirmed our previous finding (*1*) of a racemization of the α-amino acid. We suggest that this racemization occurs at the hydantoin stage, which agrees with previous work (*4*), whereas the *N*-carboxy-amino acid anhydride is refractory to racemization (*3*).

Our findings establish the catabolic segment of a peptide cycle. Both the anabolic and the catabolic segments of the peptide cycle are driven by energy coupling with a net conversion of CO to CO_2. The mechanisms of both energy couplings are analogous, proceeding through analogous five-membered rings (*N*-carboxy-amino acid anhydride or imide, respectively). This conversion is an oxidation reaction. The corresponding oxidizing agent is seen in the colloidal system $(Fe^{II},Ni^{II})S$-CO, which is present in great excess. Its reduction may proceed stoichiometrically or catalytically with H^+ and/or CO as terminal oxidant. The redox energy driving the peptide cycle is converted into group activation energy in (B) and (E). The redox energy flow is normally inhibited, but it is here catalyzed by the peptide cycle. This is the mark of a metabolism.

Our results are compatible with the theory of a chemoautotrophic origin of life (*5*, *6*) in the presence of CO-laden volcanic exhalations. For the heterotrophic origin of life in a prebiotic broth, it has been suggested that hydantoin derivatives of α-amino acids (not of peptides) formed by dehydrating ring closure of *N*-carbamoyl-amino acids and led to prebiotic peptides and to the emergence of an Ur-hydantoinase (*7*). According to our results, hydantoins are not precursors for the synthesis of peptides but rather are intermediates in the breakdown of peptides. This is yet another example of the differences between these two theories.

The anabolic and catabolic segments of the peptide cycle operate simultaneously and under exactly the same conditions. This means that in a primordial metabolism the constituents of the peptide cycle exist under steady-state conditions. In extant organisms, peptides or proteins are synthesized as well as degraded. This is a precondition for metabolic control and for preventing the cellular metabolism from being choked by peptides. We suggest that the primordial peptide cycle may have continued to function until after the onset of cellularization.

Because the constituents of the primordial peptide cycle are continuously formed and degraded, they form a dynamic chemical library that scans the space of structural possibilities. This library may well have been self-selecting, because the constituents may be differentially stabilized by bonding as ligands to transition-metal centers, and early evolution may be seen as proceeding by positive ligand feedback into the catalytic transition-metal centers of the metabolism.

The new CO-driven peptide degradation may be used for a one-pot sequencing of peptides or proteins (at least their N-terminal segments). The reaction may also be used for converting a mixture of α-amino acids into a chemical library for screening.

The hydantoin derivative resulting from a glycylpeptide is related to the imidazol ring of uric acid. This opens a surprise connection between the origin of peptides and a possible origin of purines, which by extension would support the notion of a coevolution of peptides (proteins) and nucleic acids. The demonstrated hydrolysis of the hydantoin derivative with (Fe,Ni)S may be seen as the evolutionary precursor of the reaction of hydantoinase, a metal-dependent enzyme (*4*). The demonstrated hydrolysis of the urea derivative with (Fe,Ni)S may be seen as the evolutionary precursor of the reaction of the Ni-enzyme urease (*8*). If this notion is correct, these enzymes and their metal dependence may well be extant echoes from the distant past of life.

References and Notes

1. C. Huber, G. Wächtershäuser, *Science* **281**, 670 (1998).
2. Materials and methods are available as supporting material on *Science* Online.
3. H. R. Kricheldorf, *α-Aminoacid-N-Carboxy Anhydrides and Related Heterocycles: Syntheses, Properties, Peptide Synthesis, Polymerization* (Springer Verlag, Berlin, 1987).
4. C. Syldatk *et al.*, *Appl. Microbiol. Biotechnol.* **51**, 293 (1999).
5. G. Wächtershäuser, *Microbiol. Rev.* **52**, 452 (1988).
6. C. Huber, G. Wächtershäuser, *Science* **276**, 245 (1997).
7. J. Taillades *et al.*, *Origins Life Evol. Biosph.* **28**, 61 (1998).
8. E. Jabri *et al.*, *Science* **268**, 998 (1995).

9. This work was funded by Deutsche Forschungsgemeinschaft (WA-983/1-4). We thank A. Bacher for providing the laboratory facilities for carrying out this work and for continued support, B. Cordes for HPLC-MS, and M. Schulte-Bockholt for laboratory assistance.

Supporting Online Material

www.sciencemag.org/cgi/content/full/301/5635/938/DC1
Materials and Methods
Figs. S1 and S2

6 May 2003; accepted 1 July 2003

A Quantum Laser Pointer

Nicolas Treps,[1,2]* Nicolai Grosse,[1] Warwick P. Bowen,[1] Claude Fabre,[2] Hans-A. Bachor,[1] Ping Koy Lam[1]

The measurement sensitivity of the pointing direction of a laser beam is ultimately limited by the quantum nature of light. To reduce this limit, we have experimentally produced a quantum laser pointer, a beam of light whose direction is measured with a precision greater than that possible for a usual laser beam. The laser pointer is generated by combining three different beams in three orthogonal transverse modes, two of them in a squeezed-vacuum state and one in an intense coherent field. The result provides a demonstration of multichannel spatial squeezing, along with its application to the improvement of beam positioning sensitivity and, more generally, to imaging.

Measuring the pointing direction of a laser beam is one of the most direct, practical, and sensitive applications of light. It is used to detect with high sensitivity various weak physical effects such as spatial electro-optical or magneto-optical variations, refractive index gradients, the motion of single macromolecules, or the displacements of cantile-

vers in surface microscopes (*1*). On the other hand, this type of measurement, done at the quantum level, is one of the simplest systems for the study of the quantum properties of optical imaging (*2*). We demonstrated experimentally the limit to position measurements imposed by the quantum aspects of a usual laser beam, in which the photons are randomly distributed within the transverse plane. We showed how this standard quantum limit can be reduced using nonclassical light with specially designed spatial quantum correlations in both spatial coordinates (x and y), which allows a cancellation of the quantum noise in the position measurement. This device, termed a "quantum laser pointer," may be used to improve the sensitivity of a wide range of optical instruments. This is also a demonstration of a multichannel nonclassical beam of light: The photons are spatially ordered in the two transverse dimensions.

The most commonly used device to measure the position of the center of a beam of light is a split detector, that is, a detector with two or more separated areas. The difference between the photocurrents delivered by these areas is proportional to the displacement of the beam relative to the detector. Because we wanted to measure the two coordinates of the beam's center, we used a quadrant detector (Fig. 1). The two currents

$$I_x = (I_a + I_b) - (I_c + I_d),$$
$$I_y = (I_a + I_c) - (I_b + I_d) \qquad (1)$$

(where I_a, I_b, I_c, and I_d designate measurements in each quadrant) are proportional, respectively, to the horizontal and vertical position of the laser beam in the small displacement regime.

Instead of the average position of the beam, which is difficult to measure because of low-frequency vibrations and air index fluctuations, we considered and measured oscillations of the beam position with ultrasmall amplitude d_{mod} at high temporal frequencies Ω ($\Omega >$ 1 Mhz). The ultimate limit of the position measurement is given by quantum mechanics: The noise in the measurement arising from the random arrival time of the photons on the detector is responsible for a lower limit to the amplitude d that can be measured with a coherent beam (i.e., a perfect usual laser beam) and corresponds to a signal-to-noise ratio equal to 1 (*3*). This quantum noise, or shot noise, limit is given, in the case of a TEM_{00} (transverse electromagnetic) beam, by

$$d_{QNL} \approx \sqrt{\frac{\pi}{8}}\frac{w_0}{\sqrt{N}} \qquad (2)$$

where w_0 is the waist of the Gaussian beam and N is the number of photons detected per measurement time interval Δt. To demonstrate this limit experimentally, we first measured the quantum noise $n(\Omega)$ with no modulation, using standard quantum optics techniques (*4*), and then added a very small modulation of the beam position $d(\Omega)$. The recorded signal contains both the actual displacement signal and the quantum noise. This noise can be reduced by averaging the traces over a long time, but at the expense of fast response time. We therefore chose a fixed integration time, Δt. We can be sure, with a reasonable degree of confidence, that the signal is due to an actual beam oscillation, rather than to a large fluctuation of the background noise, when the total signal—displacement and noise—is larger than the quantum noise alone. For example, we can choose as the smallest detectable amplitude that value for which the two traces differ by 3 standard deviations.

To determine the oscillation amplitude at a defined analysis frequency Ω, we used a spectrum analyzer, which demodulates the signal and measures the power spectral density. It displays the value for $n(\Omega)^2 + d(\Omega)^2$ on a logarithmic *dB* scale (Fig. 2A). We chose as the detection time Δt = 10 μs and set the resolution bandwidth (RBW) and video bandwidth (VBW) of the spectrum ana-

[1]Australian Research Council Centre of Excellence for Quantum-Atom Optics, the Australian National University, Canberra ACT 0200, Australia. [2]Laboratoire Kastler Brossel, Université Pierre et Marie Curie, case 74, 75252 Paris cedex 05, France.

*To whom correspondence should be addressed. E-mail: nicolas.treps@spectro.jussieu.fr

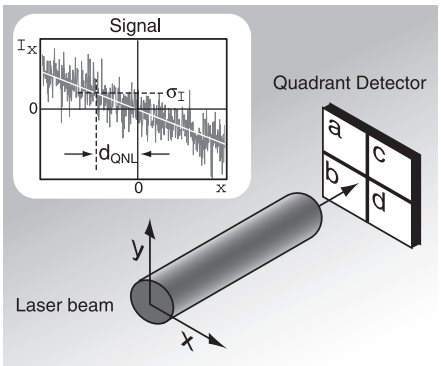

Fig. 1. Measurement of laser beam direction. A laser beam is incident on a quadrant detector. Simple arithmetic operations are performed on the four photo currents to produce signals I_x and I_y, which are proportional to the displacement in the horizontal and vertical axes, respectively. An example signal for I_x is plotted. The standard deviation of the signal σ_I defines the quantum noise limited displacement d_{QNL}.

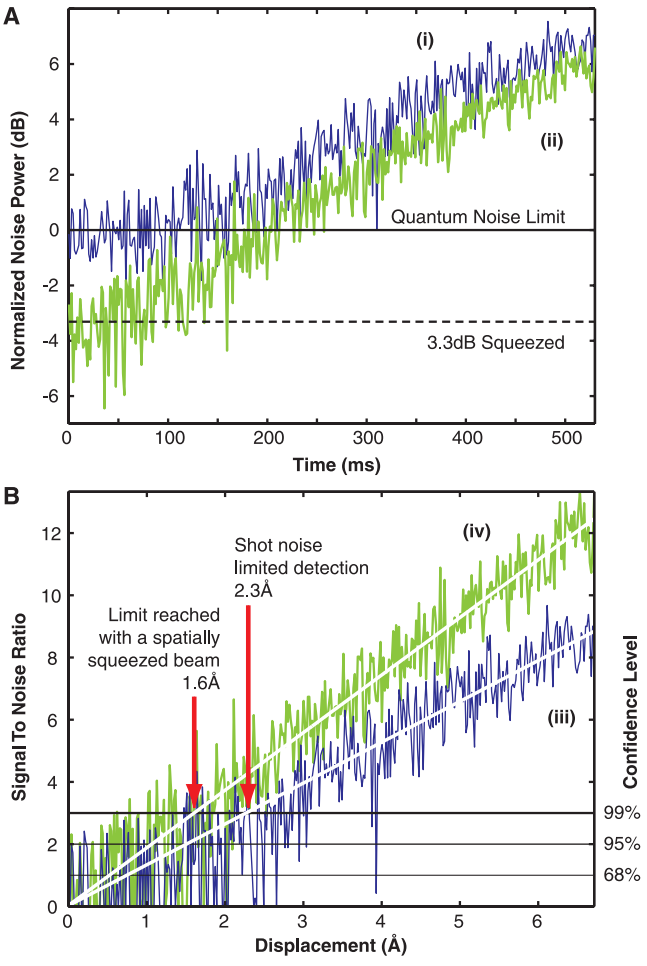

Fig. 2. (**A**) Measurement of horizontal displacement signal ramped up in time, with (i) coherent beams and (ii) spatially squeezed beams. Both radio-frequency spectrum analyzer traces are the averages of 20 runs with VBW = RBW = 1 kHz. The observed noise reduction of the squeezed beams measurement is 3.3 ± 0.2 dB. (**B**) Data from (A) processed to show signal-to-noise improvement (left vertical axis) plotted against the inferred displacement. Traces (iii) and (iv) show the results from data (i) and (ii), respectively. The squeezing translates into an increase in displacement sensitivity. Choosing a 99% confidence level (right vertical axis), the smallest displacement detectable improved from 2.3 to 1.6 Å.

lyzer to 1 kHz. We used a mirror mounted on a piezo-electric transducer to perform the oscillation. The modulation amplitude d_{mod} was slowly increased over time. The upper curve corresponds to the measurement performed with a coherent state and is the best measurement that can be achieved with classical means. The lower curve corresponds to the same measurement but with the nonclassical beam, called a "spatially squeezed" beam, that we produced as described below. The signal differs from the background noise for a modulation amplitude, which is greater for the coherent beam than for the spatially squeezed beam. In Fig. 2B, the same data are normalized to the respective noise levels, both for a usual laser and for a spatially squeezed beam. The vertical axis is now the difference between the measured signal and the noise with no displacement, and the traces for the coherent and the spatially squeezed beams are superimposed. In the case of the spatially squeezed light, the average of the signal trace crosses the threshold of confidence, set here at 3 standard deviations, for a smaller oscillation amplitude. We found a corresponding oscillation amplitude of 1.6 Å and an improvement by a factor of 1.5 compared with the standard quantum noise limit. Because both traces increase linearly with d_{mod}, this result is independent of the choice of confidence level. Most important, we have achieved such an improvement for two simultaneous measurements performed on the beam, namely the oscillation amplitudes in two orthogonal directions.

Let us consider a beam incident and centered on a quadrant detector. As in (3), we describe the electric field operator by

$$\hat{E}(x, y) = \sum_i \hat{a}_i u_i(x, y) \qquad (3)$$

where (x, y) are the transverse coordinates, $[u_i]$ is a complete basis of transverse modes, and $\hat{a}_i$ is the corresponding annihilation operator. Because the displacement to be measured is very small compared with the diameter of the beam, the noise on the signals I_x and I_y of Eq. 1 can be calculated when the beam is exactly centered, that is, when

$$\langle \int_{x<0} \hat{E}^\dagger \hat{E}\, dxdy \rangle = \langle \int_{x>0} \hat{E}^\dagger \hat{E}\, dxdy \rangle \text{ and}$$

$$\langle \int_{y<0} \hat{E}^\dagger \hat{E}\, dxdy \rangle = \langle \int_{y>0} \hat{E}^\dagger \hat{E}\, dxdy \rangle \qquad (4)$$

We chose the transverse modes basis such that the first transverse mode u_0 has the shape of the input beam, $u_0(x,y) = \langle \hat{E}(x,y) \rangle / \| E(x,y) \|$. Then we defined two "flipped modes," u_1 and u_2, such that $u_1(x,y) = -u_0(x,y)$ for $x < 0$, $u_1(x,y) = u_0(x,y)$ for $x > 0$, $u_2(x,y) = -u_0(x,y)$ for $y < 0$, and $u_2(x,y) = u_0(x,y)$ for $y > 0$. The important point is that Eq. 4 ensures that u_0, u_1, and u_2 are orthonormal and hence can actually be the beginning of a transverse-mode basis. It can be shown that the noise in the horizontal and vertical measurements arises only from the noise of u_1 and u_2, respectively (*5*). Hence, both measurements can be improved if and only if both modes are vacuum-squeezed states. These considerations show that to improve simultaneously two independent measurements on a light beam, it is necessary to use a multimode transverse beam containing two squeezed states in the mode u_1 and u_2, that is, a true spatially multimode squeezed beam (*6*). This analysis can be extended to an arbitrary number of independent measurements, each measurement being a channel in an information theory point of view: To improve an n-channel measurement beyond the standard quantum limit, one needs to use n squeezed states in appropriate modes. This bears a strong similarity to the quantum study of superresolution (*7*).

To construct our quantum laser pointer, three beams are necessary, two in squeezed-vacuum states and the third in an intense coherent state. These three beams have to be mixed, avoiding any losses for at least the two squeezed beams, because that would destroy the squeezing. In our setup (Fig. 3), the two highly squeezed beams (about 4 dB) are produced by two optical parametric amplifiers (OPAs) (*8*) driven by one laser. We chose an unusual spatial mode distribution: The transverse mode u_0 (corresponding to the bright coherent state) is the horizontally flipped mode of a TEM_{00} mode. Hence, the first squeezed beam (u_1) is in the TEM_{00} mode and the second squeezed beam (u_2) is in a "doubly flipped" TEM_{00} mode, as shown in the phase distribution maps in Fig. 3. The transverse modes are produced with optical wave plates made from birefringent half wave plates that were assembled at the appropriate $\pi/2$ angle. We used either two singly flipped wave plates or a four-quadrant wave plate. The mixing is achieved with a ring optical cavity. The TEM_{00} squeezed beam can be transmitted with nearly 100% efficiency in the case of an impedance-matched cavity. Because we chose a transversally nondegenerate cavity, the other squeezed beam, which is in a transverse mode orthogonal to the TEM_{00} mode, is reflected at the output mirror of the cavity and then perfectly mixed with the first squeezed beam. The cavity had a finesse of around 35, and we measured an efficiency of >95% for the transmitted beam and >94% for the reflected beam. The limit in efficiency came essentially from the imperfections of the OPA beam shape compared with a TEM_{00} mode. This technique for mixing the two beams

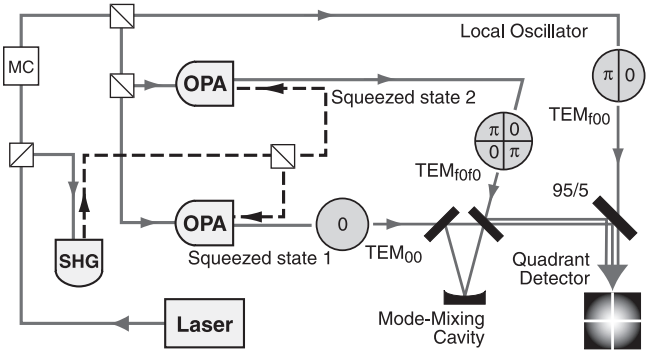

Fig. 3. Schematic of the experiment. SHG, second harmonic generator; OPA, optical parametric amplifier; MC, mode cleaner; 95/5, beam splitter with 95% reflectivity; TEM_{00}, squeezed TEM_{00} mode used for improving the horizontal measurement; TEM_{f0f0}, squeezed TEM_{f0f0} mode used for improving the vertical measurement; TEM_{f00}, coherent TEM_{f00} mode used as a local oscillator. Dotted lines, 532 nm light; solid lines, 1064 nm light.

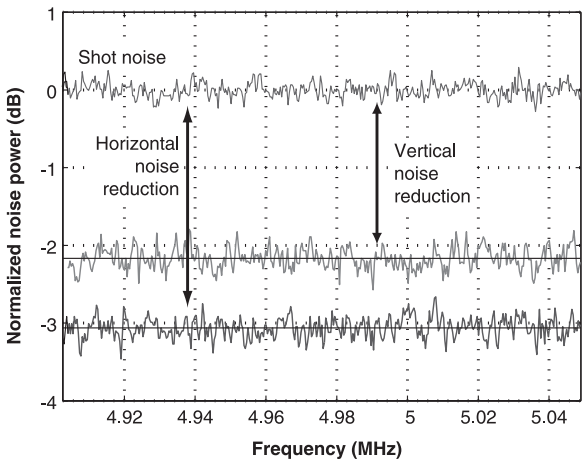

Fig. 4. Measured spectra showing the noise reductions in both horizontal and vertical measurements. The top trace corresponds to the quantum noise limit (QNL), whereas the two lower ones correspond to the noise in the vertical and the horizontal measurements done with a spatially squeezed beam. The noise spectra are normalized to 0 dB = QNL.

had, to our knowledge, never been implemented before and can be extended to a wide range of applications. In particular, it can be used to mix any two orthogonal transverse modes. Finally, the resulting beam is mixed with the coherent beam on a 95%/5% beam splitter as in (*5*).

The experiment was performed in a fully locked configuration, stable for at least 10 minutes. The detection was performed with a quadrant detector, each of the quadrants having a high quantum efficiency (more than 90%), and the corresponding electronic amplifiers were optimized to ensure their exact balance (*9*). The four individual photocurrents were combined to measure the quantities I_x and I_y of Eq. 1. A spectrum analyzer was used to perform the demodulation and obtain the detection at 4.3 MHz. A first experiment, without any modulation, showed the amount of noise reduction we could obtain (Fig. 4). We achieved simultaneously 3.05 ± 0.1 dB of horizontal noise reduction and 2.0 ± 0.1 dB of vertical noise reduction. The configuration used here is scalable, and it is possible to increase the number of independent modes with a slight variation of the layout. From a quantum information point of view, each transverse mode is an independent communication channel, and the usual quantum communication proposals can be extended to the multichannel configuration (*10*, *11*). This same beam of light was used to perform the displacement measurement described above.

Our experiment can be considered with equal interest from different points of view. On the fundamental side, it is now possible to experimentally mix several nonclassical beams in orthogonal transverse modes, thereby producing multimode spatially squeezed beams. This ability is of major importance in the field of quantum imaging. On the quantum information side, this experiment opens the way to the use of multimode light in the parallel processing of quantum information. Finally, this experiment clearly demonstrates the practical applicability of spatial squeezing to displacement measurements. As a major advance, this experiment overcomes most of the technical obstacles. In particular, we can avoid losses in the mixing of the transverse modes.

Our technique can be used to improve the measurement of a displacement induced by interaction with a physical system, as discussed in (*12*), even if this interaction introduces losses. Indeed, it will be possible to mix the coherent state with the squeezed states after the interaction, and without losses. Real applications will follow after the production of easy-to-use, efficient sources of squeezed light.

References and Notes

1. Tim J. Senden, *Current Opinion in Colloid and Interface Science* **6**, 95 (2001).
2. L. A. Lugiato, A. Gatti, E. Brambilla, *J. Opt. B Quantum Semiclass. Opt.* **4**, S176 (2002).
3. C. Fabre, J. B. Fouet, A. Maître, *Optics Letters* **25**, 76 (1999).
4. H.-A. Bachor, *A Guide to Experiments in Quantum Optics* (Wiley-VCH, Weinheim, Germany, 1998).
5. N. Treps *et al.*, *Phys. Rev. Letters* **88**, 203601 (2002).
6. M. I. Kolobov, *Rev. Mod. Phys.* **71**, 1539 (1999).
7. M. I. Kolobov, C. Fabre, *Phys. Rev. Lett.* **85**, 3789 (2000).
8. W. P. Bowen, R. Schnabel, H.-A. Bachor, P. K. Lam, *Phys. Rev. Lett.* **88**, 093601 (2002).
9. M. Martinelli *et al.*, *Phys. Rev. A* **67**, 023808 (2003).
10. I. V. Sokolov, M. I. Kolobov, A. Gatti, L. A. Lugiato, *Opt. Comm.* **193**, 174 (2001).
11. I. V. Sokolov, internal communication within the European Network on Quantum Imaging (QUANTIM) on the possibility of multimode dense coding.
12. C. Boccara, D. Fournier, J. Badoz, *Appl. Phys. Lett.* **36**, 130 (1980).

13. This work was carried out as part of the Australian Research Council Centre of Excellence Program. It was funded by the Australian Research Council and supported by the Laboratoire Kastler Brossel as part of QUANTIM, contract IST-2000-26019. We thank the Commonwealth Scientific and Industrial Research Organisation (Lindfield, Australia) for the precise making of the wave plates; B.C. Buchler and R. Schnabel for their valuable contributions, in particular to the design, construction, and optimization of the two OPAs; and A. Maître for invaluable discussions.

6 May 2003; accepted 9 July 2003

Electrical Manipulation of Magnetization Reversal in a Ferromagnetic Semiconductor

D. Chiba,[1] M. Yamanouchi,[1] F. Matsukura,[1] H. Ohno[1,2]*

We report electrical manipulation of magnetization processes in a ferromagnetic semiconductor, in which low-density carriers are responsible for the ferromagnetic interaction. The coercive force H_C at which magnetization reversal occurs can be manipulated by modifying the carrier density through application of electric fields in a gated structure. Electrically assisted magnetization reversal, as well as electrical demagnetization, has been demonstrated through the effect. This electrical manipulation offers a functionality not previously accessible in magnetic materials and may become useful for reversing magnetization of nanoscale bits for ultrahigh-density information storage.

Magnetization reversal is a fundamental process for writing information, or bits, onto magnetic materials used in data storage, and is generally done by applying magnetic fields locally to the magnetic material. In order to realize higher data density per unit area, the magnetic energy density of the material has to be increased to make the nanometer-scale magnetic bits stable against thermal fluctuations, which at its limit pushes the required magnetic fields for writing too high to generate. Manipulation of magnetization reversal by other means has thus become an important challenge for magnetic information storage (*1*–*5*). We show that electrical manipulation of the magnetization processes is possible in a semiconducting ferromagnetic material and demonstrate electrically assisted magnetization reversal, as well as electrical demagnetization.

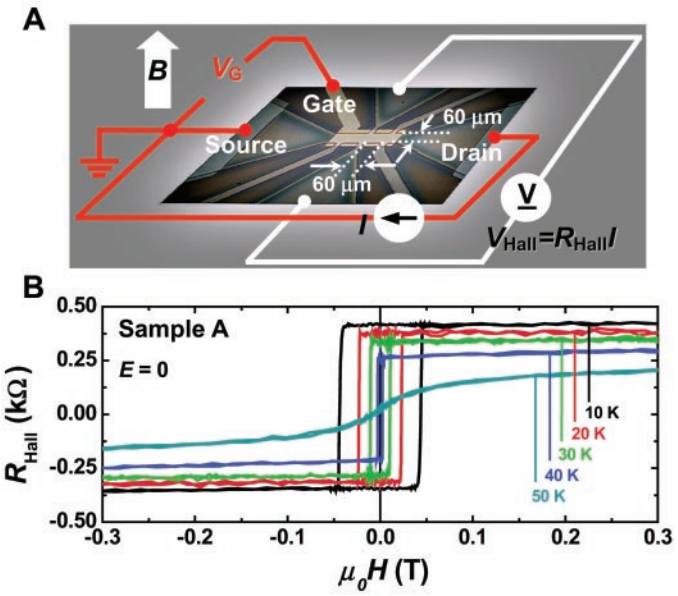

Fig. 1. (**A**) Hall bar–shaped field effect transistor having a ferromagnetic semiconductor (In,Mn)As channel. To probe the magnetization M of the channel, Hall resistance $R_{Hall} = V_{Hall}/I$ proportional to the channel magnetization is measured. (**B**) Temperature dependence of R_{Hall} ($\propto M$) versus magnetic field $\mu_0 H$ curves with square-shaped hysteresis up to temperatures below 50 K in sample A. Sample A has a ferromagnetic transition temperature of 52 K. No electric field is applied ($E = 0$). Magnetic field sweep rate is 3.7 mT/min.